Tau Decays with Neutral Kaons

The OPAL Collaboration

Abstract

The branching ratio of the τ lepton to a neutral kaon meson is measured from a sample of approximately 200,000 τ decays recorded by the OPAL detector at centre-of-mass energies near the Z^0 resonance. The measurement is based on two samples which identify one-prong τ decays with K^0_L and K^0_S mesons. The combined branching ratios are measured to be

$$
\begin{aligned}
B(\tau^- \to \pi^- \overline{K}^0 \nu_\tau) &= (9.33 \pm 0.68 \pm 0.49) \times 10^{-3}, \\
B(\tau^- \to \pi^- \overline{K}^0 [\geq 1\pi^0] \nu_\tau) &= (3.24 \pm 0.74 \pm 0.66) \times 10^{-3}, \\
B(\tau^- \to K^- K^0 [\geq 0\pi^0] \nu_\tau) &= (3.30 \pm 0.55 \pm 0.39) \times 10^{-3},
\end{aligned}
$$

where the first error is statistical and the second systematic.

(To be submitted to European Physical Journal C)

The OPAL Collaboration

G. Abbiendi[2], K. Ackerstaff[8], P.F. Akesson[3], G. Alexander[23], J. Allison[16], K.J. Anderson[9], S. Arcelli[17], S. Asai[24], S.F. Ashby[1], D. Axen[29], G. Azuelos[18,a], I. Bailey[28], A.H. Ball[8], E. Barberio[8], R.J. Barlow[16], J.R. Batley[5], S. Baumann[3], T. Behnke[27], K.W. Bell[20], G. Bella[23], A. Bellerive[9], S. Bentvelsen[8], S. Bethke[14,i], S. Betts[15], O. Biebel[14,i], A. Biguzzi[5], I.J. Bloodworth[1], P. Bock[11], J. Böhme[14,h], O. Boeriu[10], D. Bonacorsi[2], M. Boutemeur[33], S. Braibant[8], P. Bright-Thomas[1], L. Brigliadori[2], R.M. Brown[20], H.J. Burckhart[8], P. Capiluppi[2], R.K. Carnegie[6], A.A. Carter[13], J.R. Carter[5], C.Y. Chang[17], D.G. Charlton[1,b], D. Chrisman[4], C. Ciocca[2], P.E.L. Clarke[15], E. Clay[15], I. Cohen[23], J.E. Conboy[15], O.C. Cooke[8], J. Couchman[15], C. Couyoumtzelis[13], R.L. Coxe[9], M. Cuffiani[2], S. Dado[22], G.M. Dallavalle[2], S. Dallison[16], R. Davis[30], A. de Roeck[8], P. Dervan[15], K. Desch[27], B. Dienes[32,h], M.S. Dixit[7], M. Donkers[6], J. Dubbert[33], E. Duchovni[26], G. Duckeck[33], I.P. Duerdoth[16], P.G. Estabrooks[6], E. Etzion[23], F. Fabbri[2], A. Fanfani[2], M. Fanti[2], A.A. Faust[30], L. Feld[10], P. Ferrari[12], F. Fiedler[27], M. Fierro[2], I. Fleck[10], A. Frey[8], A. Fürtjes[8], D.I. Futyan[16], P. Gagnon[12], J.W. Gary[4], G. Gaycken[27], C. Geich-Gimbel[3], G. Giacomelli[2], P. Giacomelli[2], D.M. Gingrich[30,a], D. Glenzinski[9], J. Goldberg[22], W. Gorn[4], C. Grandi[2], K. Graham[28], E. Gross[26], J. Grunhaus[23], M. Gruwé[27], C. Hajdu[31] G.G. Hanson[12], M. Hansroul[8], M. Hapke[13], K. Harder[27], A. Harel[22], C.K. Hargrove[7], M. Harin-Dirac[4], M. Hauschild[8], C.M. Hawkes[1], R. Hawkings[27], R.J. Hemingway[6], G. Herten[10], R.D. Heuer[27], M.D. Hildreth[8], J.C. Hill[5], P.R. Hobson[25], A. Hocker[9], K. Hoffman[8], R.J. Homer[1], A.K. Honma[8], D. Horváth[31,c], K.R. Hossain[30], R. Howard[29], P. Hüntemeyer[27], P. Igo-Kemenes[11], D.C. Imrie[25], K. Ishii[24], F.R. Jacob[20], A. Jawahery[17], H. Jeremie[18], M. Jimack[1], C.R. Jones[5], P. Jovanovic[1], T.R. Junk[6], N. Kanaya[24], J. Kanzaki[24], G. Karapetian[18], D. Karlen[6], V. Kartvelishvili[16], K. Kawagoe[24], T. Kawamoto[24], P.I. Kayal[30], R.K. Keeler[28], R.G. Kellogg[17], B.W. Kennedy[20], D.H. Kim[19], A. Klier[26], T. Kobayashi[24], M. Kobel[3], T.P. Kokott[3], M. Kolrep[10], S. Komamiya[24], R.V. Kowalewski[28], T. Kress[4], P. Krieger[6], J. von Krogh[11], T. Kuhl[3], M. Kupper[26], P. Kyberd[13], G.D. Lafferty[16], H. Landsman[22], D. Lanske[14], J. Lauber[15], I. Lawson[28], J.G. Layter[4], D. Lellouch[26], J. Letts[12], L. Levinson[26], R. Liebisch[11], J. Lillich[10], B. List[8], C. Littlewood[5], A.W. Lloyd[1], S.L. Lloyd[13], F.K. Loebinger[16], G.D. Long[28], M.J. Losty[7], J. Lu[29], J. Ludwig[10], A. Macchiolo[18], A. Macpherson[30], W. Mader[3], M. Mannelli[8], S. Marcellini[2], T.E. Marchant[16], A.J. Martin[13], J.P. Martin[18], G. Martinez[17], T. Mashimo[24], P. Mättig[26], W.J. McDonald[30], J. McKenna[29], E.A. Mckigney[15], T.J. McMahon[1], R.A. McPherson[28], F. Meijers[8], P. Mendez-Lorenzo[33], F.S. Merritt[9], H. Mes[7], I. Meyer[5], A. Michelini[2], S. Mihara[24], G. Mikenberg[26], D.J. Miller[15], W. Mohr[10], A. Montanari[2], T. Mori[24], K. Nagai[8], I. Nakamura[24], H.A. Neal[12,f], R. Nisius[8], S.W. O'Neale[1], F.G. Oakham[7], F. Odorici[2], H.O. Ogren[12], A. Okpara[11], M.J. Oreglia[9], S. Orito[24], G. Pásztor[31], J.R. Pater[16], G.N. Patrick[20], J. Patt[10], R. Perez-Ochoa[8], S. Petzold[27], P. Pfeifenschneider[14], J.E. Pilcher[9], J. Pinfold[30], D.E. Plane[8], B. Poli[2], J. Polok[8], M. Przybycień[8,d], A. Quadt[8], C. Rembser[8], H. Rick[8], S.A. Robins[22], N. Rodning[30], J.M. Roney[28], S. Rosati[3], K. Roscoe[16], A.M. Rossi[2], Y. Rozen[22], K. Runge[10], O. Runolfsson[8], D.R. Rust[12], K. Sachs[10], T. Saeki[24], O. Sahr[33], W.M. Sang[25], E.K.G. Sarkisyan[23], C. Sbarra[28], A.D. Schaile[33], O. Schaile[33], P. Scharff-Hansen[8], J. Schieck[11], S. Schmitt[11], A. Schöning[8], M. Schröder[8], M. Schumacher[3], C. Schwick[8], W.G. Scott[20], R. Seuster[14,h], T.G. Shears[8], B.C. Shen[4], C.H. Shepherd-Themistocleous[5], P. Sherwood[15], G.P. Siroli[2], A. Skuja[17], A.M. Smith[8], G.A. Snow[17], R. Sobie[28], S. Söldner-Rembold[10,e], S. Spagnolo[20], M. Sproston[20], A. Stahl[3], K. Stephens[16], K. Stoll[10], D. Strom[19], R. Ströhmer[33], B. Surrow[8], S.D. Talbot[1], P. Taras[18], S. Tarem[22], R. Teuscher[9], M. Thiergen[10], J. Thomas[15],

M.A. Thomson[8], E. Torrence[8], S. Towers[6], T. Trefzger[33], I. Trigger[18], Z. Trócsányi[32,g],
E. Tsur[23], M.F. Turner-Watson[1], I. Ueda[24], R. Van Kooten[12], P. Vannerem[10], M. Verzocchi[8],
H. Voss[3], F. Wäckerle[10], D. Waller[6], C.P. Ward[5], D.R. Ward[5], P.M. Watkins[1], A.T. Watson[1],
N.K. Watson[1], P.S. Wells[8], T. Wengler[8], N. Wermes[3], D. Wetterling[11] J.S. White[6],
G.W. Wilson[16], J.A. Wilson[1], T.R. Wyatt[16], S. Yamashita[24], V. Zacek[18], D. Zer-Zion[8]

[1]School of Physics and Astronomy, University of Birmingham, Birmingham B15 2TT, UK
[2]Dipartimento di Fisica dell' Università di Bologna and INFN, I-40126 Bologna, Italy
[3]Physikalisches Institut, Universität Bonn, D-53115 Bonn, Germany
[4]Department of Physics, University of California, Riverside CA 92521, USA
[5]Cavendish Laboratory, Cambridge CB3 0HE, UK
[6]Ottawa-Carleton Institute for Physics, Department of Physics, Carleton University, Ottawa, Ontario K1S 5B6, Canada
[7]Centre for Research in Particle Physics, Carleton University, Ottawa, Ontario K1S 5B6, Canada
[8]CERN, European Organisation for Particle Physics, CH-1211 Geneva 23, Switzerland
[9]Enrico Fermi Institute and Department of Physics, University of Chicago, Chicago IL 60637, USA
[10]Fakultät für Physik, Albert Ludwigs Universität, D-79104 Freiburg, Germany
[11]Physikalisches Institut, Universität Heidelberg, D-69120 Heidelberg, Germany
[12]Indiana University, Department of Physics, Swain Hall West 117, Bloomington IN 47405, USA
[13]Queen Mary and Westfield College, University of London, London E1 4NS, UK
[14]Technische Hochschule Aachen, III Physikalisches Institut, Sommerfeldstrasse 26-28, D-52056 Aachen, Germany
[15]University College London, London WC1E 6BT, UK
[16]Department of Physics, Schuster Laboratory, The University, Manchester M13 9PL, UK
[17]Department of Physics, University of Maryland, College Park, MD 20742, USA
[18]Laboratoire de Physique Nucléaire, Université de Montréal, Montréal, Quebec H3C 3J7, Canada
[19]University of Oregon, Department of Physics, Eugene OR 97403, USA
[20]CLRC Rutherford Appleton Laboratory, Chilton, Didcot, Oxfordshire OX11 0QX, UK
[22]Department of Physics, Technion-Israel Institute of Technology, Haifa 32000, Israel
[23]Department of Physics and Astronomy, Tel Aviv University, Tel Aviv 69978, Israel
[24]International Centre for Elementary Particle Physics and Department of Physics, University of Tokyo, Tokyo 113-0033, and Kobe University, Kobe 657-8501, Japan
[25]Institute of Physical and Environmental Sciences, Brunel University, Uxbridge, Middlesex UB8 3PH, UK
[26]Particle Physics Department, Weizmann Institute of Science, Rehovot 76100, Israel
[27]Universität Hamburg/DESY, II Institut für Experimental Physik, Notkestrasse 85, D-22607 Hamburg, Germany
[28]University of Victoria, Department of Physics, P O Box 3055, Victoria BC V8W 3P6, Canada
[29]University of British Columbia, Department of Physics, Vancouver BC V6T 1Z1, Canada
[30]University of Alberta, Department of Physics, Edmonton AB T6G 2J1, Canada
[31]Research Institute for Particle and Nuclear Physics, H-1525 Budapest, P O Box 49, Hungary
[32]Institute of Nuclear Research, H-4001 Debrecen, P O Box 51, Hungary

[33] Ludwigs-Maximilians-Universität München, Sektion Physik, Am Coulombwall 1, D-85748 Garching, Germany

[a] and at TRIUMF, Vancouver, Canada V6T 2A3
[b] and Royal Society University Research Fellow
[c] and Institute of Nuclear Research, Debrecen, Hungary
[d] and University of Mining and Metallurgy, Cracow
[e] and Heisenberg Fellow
[f] now at Yale University, Dept of Physics, New Haven, USA
[g] and Department of Experimental Physics, Lajos Kossuth University, Debrecen, Hungary
[h] and MPI München
[i] now at MPI für Physik, 80805 München.

1 Introduction

The large samples of Z^0 events collected at e^+e^- colliders over the past ten years have made it possible to study resonance dynamics and test low energy QCD using the decays of τ leptons to kaons. In this paper, measurements of the branching ratios of the $\tau^- \to \pi^-\overline{K}^0\nu_\tau$, $\tau^- \to \pi^-\overline{K}^0[\geq 1\pi^0]\nu_\tau$ and $\tau^- \to K^-K^0[\geq 0\pi^0]\nu_\tau$ decay modes are presented.[1] These measurements are based on two samples that identify τ decays with K^0_L and K^0_S mesons. The K^0_L mesons are identified by their one-prong nature accompanied by a large deposition of energy in the hadron calorimeter while the K^0_S mesons are identified through their decay into two charged pions. The selected number of $\tau^- \to \pi^-\overline{K}^0K^0\nu_\tau$ decays is very small and is treated as background in this analysis.

The results presented here are extracted from the data collected between 1991 and 1995 at energies close to the Z^0 resonance, corresponding to an integrated luminosity of 163 pb^{-1}, with the OPAL detector at LEP. A description of the OPAL detector can be found in [1]. The performance and particle identification capabilities of the OPAL jet chamber are described in [2]. The τ pair Monte Carlo samples used in this analysis are generated using the KORALZ 4.0 package [3]. The dynamics of the τ decays are simulated with the Tauola 2.4 decay library [4]. The Monte Carlo events are then passed through the OPAL detector simulation [5].

2 Selection of $\tau^+\tau^-$ events

The procedure used to select $Z^0 \to \tau^+\tau^-$ events is identical to that described in previous OPAL publications [6, 7]. The decay of the Z^0 produces two back-to-back taus. The taus are highly relativistic so that the decay products are strongly collimated. As a result it is convenient to treat each τ decay as a jet, where charged tracks and clusters are assigned to cones of half-angle $35°$ [6, 7]. In order to avoid regions of non-uniform calorimeter response, the two τ jets are restricted to the barrel region of the OPAL detector by requiring that the average polar angle[2] of the two jets satisfies $\overline{|cos\theta|} < 0.68$. The level of contamination from multihadronic events ($e^+e^- \to q\bar{q}$) is significantly reduced by requiring not more than six tracks and ten electromagnetic clusters per event. Bhabha ($e^+e^- \to e^+e^-$) and muon pair ($e^+e^- \to \mu^+\mu^-$) events are removed by rejecting events where the total electromagnetic energy and the scalar sum of the track momenta are close to the centre-of-mass energy. Two-photon events, $e^+e^- \to (e^+e^-)e^+e^-$ or $e^+e^- \to (e^+e^-)\mu^+\mu^-$, are removed by rejecting events which have little visible energy in the electromagnetic calorimeter and a large acollinearity angle[3] between the two jets.

A total of 100925 events are selected for the K^0_L sample and 85789 events are selected for the K^0_S sample from the 1991-1995 data set. The different number of $\tau^+\tau^-$ events in the two

---

[1]Charge conjugation is implied throughout this paper.

[2]In the OPAL coordinate system the e^- beam direction defines the $+z$ axis, and the centre of the LEP ring defines the $+x$ axis. The polar angle θ is measured from the $+z$ axis, and the azimuthal angle ϕ is measured from the $+x$ axis.

[3]The acollinearity angle is the supplement of the angle between the decay products of each jet.

samples is due to different detector status requirements used in each selection. The fraction of background from non-τ sources is $(1.6 \pm 0.1)\%$ [6, 7].

3 Selection of $\tau^- \rightarrow X^- \, \overline{K}_L^0 \nu_\tau$ decays

The selection of τ decays into to a final state containing at least one K_L^0 meson follows a simple cut-based procedure. Some K_S^0 mesons will be selected in this K_L^0 selection. In particular, K_S^0 mesons that decay late in the jet chamber, the solenoid or the electromagnetic calorimeter, will be indistinguishable from K_L^0 mesons and are considered to be part of the K_L^0 signal. The Monte Carlo simulation predicts that the K^0 component identified by the K_L^0 selection is composed of 86% K_L^0 and 14% K_S^0 mesons.

First, each jet must contain exactly one track pointing to the primary vertex and its momentum divided by the beam energy (p/E_{beam}) must be less than 0.5, see fig. 1(a). This requirement removes high-momentum pion decays from the one-prong sample. In order to exclude leptonic background, there must be at least one cluster in the hadron calorimeter and the total amount of energy measured by the hadronic calorimeter within the jet must be greater than 7.5 GeV, see fig. 1(b).

The $\tau^- \rightarrow X^- \, \overline{K}_L^0 \nu_\tau$ decays will deposit on average more energy in the hadron calorimeter than most other τ decays. This property is exploited using the variable, $S_H = (E_H - p)/\sigma_H$, where E_H is the total energy deposited in the hadron calorimeter for the jet, p is the momentum of the track and $\sigma_H/E_H = 0.165 + 0.847/\sqrt{E_H}$ is the hadron calorimeter resolution. The energy is calibrated and the resolution is measured using pions from τ decays that do not interact in the electromagnetic calorimeter. Events with $S_H \geq 2.0$ are classified as $X^- \, \overline{K}_L^0$ decays, see fig. 1(c). A total of 305 candidates are selected using the above requirements. The background is estimated to be 24% from other τ decays and 6% from $e^+e^- \rightarrow q\bar{q}$ events. The primary τ background consists of $\tau^- \rightarrow \pi^- \nu_\tau$, $\tau^- \rightarrow \rho(770)^- \nu_\tau$ and $\tau^- \rightarrow a_1(1260)^- \nu_\tau$ decays.

The sample of $\tau^- \rightarrow X^- \, \overline{K}_L^0 \nu_\tau$ decays is subdivided into two sets: one in which the track is identified as a pion and another in which the track is identified as a kaon. The sample with charged pions is then passed through an additional selection which identifies those decays that include a π^0 meson. The identification of the charged hadron uses the normalized specific energy loss defined as $((dE/dx)_{\text{measured}} - (dE/dx)_{\text{expected}})/\sigma_{dE/dx}$, where $\sigma_{dE/dx}$ is the dE/dx resolution. Using this quantity, it is possible to separate charged pions and kaons at a level of 2σ in the momentum range of 2-30 GeV. The expected dE/dx is calculated using the Bethe-Bloch equation parameterised for the OPAL jet chamber [2]. The parameterisation is checked using one-prong hadronic τ decays by comparing the mean values and widths of the normalised dE/dx distributions in bins of $\beta = p/E$, with $E^2 = p^2 + m_\pi^2$. It is found that a small β-dependent correction is to be applied to the Monte Carlo. The correction shifts the mean value of the expected dE/dx by up to 10% and the widths by approximately 5%. Charged pions and kaons are separated using a dE/dx probability variable W, which is calculated from the normalized dE/dx for each particle species. These are combined into pion and kaon probabilities,

$$\begin{aligned} P_\pi &= W_\pi/(W_\pi + W_K) \\ P_K &= W_K/(W_\pi + W_K). \end{aligned}$$

The distributions of the difference $P_\pi - P_K$ is shown in fig. 2(a). A track is considered to be a pion if $P_\pi > P_K$.

A neural network algorithm is used to identify the $\tau^- \to \pi^- \overline{K}^0 \nu_\tau$ and $\tau^- \to \pi^- \overline{K}^0 [\geq 1\pi^0] \nu_\tau$ decay modes. The neural network algorithm uses 7 variables to identify the τ jets:

- The total energy of the jet in the electromagnetic calorimeter divided by the beam energy, E/E_{beam}.

- The total energy of the jet in the electromagnetic calorimeter divided by the momentum of the track, E/p.

- The number of electromagnetic clusters in the jet with an energy greater than 1 GeV.

- The minimum fraction of active lead glass blocks which together contains more than 90% of the total electromagnetic energy of the jet, F_{90}.

- The difference in the azimuthal angle between the track and the presampler signal farthest away from the track but still within the jet, ϕ_{PS}.

- The difference in theta ($\Delta\theta$) and phi ($\Delta\phi$) between the track and the vector obtained by adding together all the electromagnetic calorimeter clusters in the jet.

The variables used in the neural network and the output are shown in fig. 3. If the neural network output is larger than 0.2 then the decay is considered to contain a π^0 meson.

4 Selection of $\tau^- \to X^- \overline{K}^0_S \nu_\tau$ decays

The algorithm for identifying K^0_S candidates is similar to those used in other OPAL analyses (for example, see [9]). The algorithm begins by pairing tracks with opposite charge. Each track must have a minimum transverse momentum of 150 MeV and more than 40 out of a possible 159 hits in the jet chamber. Intersection points of track pairs in the plane perpendicular to the beam axis are considered to be secondary vertex candidates. Each secondary vertex is then required to satisfy the following criteria:

- The radial distance R_V from the secondary vertex to the primary vertex must be greater than 10 cm and less than 150 cm.

- The reconstructed momentum vector of the K^0_S candidate in the plane perpendicular to the beam axis must point to the beam axis within $1°$.

- If R_V is between 30 and 150 cm (i.e. the secondary vertex is inside the jet chamber volume), then the radius of the first jet chamber hit associated with either of the two tracks (R_1) must satisfy $R_V - R_1 < 5$ cm.

- If R_V is between 10 and 30 cm (not inside the jet chamber volume), then the impact parameter of the track is required to exceed 1 mm.

- The invariant mass of the pair of tracks, assuming both tracks to be electrons from a photon conversion, is required to be greater than 100 MeV.

The τ jet is required to have at least one K_S^0 candidate. If there is more than one candidate then only the secondary vertex with an invariant mass closest to the true K_S^0 mass is retained. In addition, each jet is required to have only one additional track, called the primary track.

A number of additional criteria are applied to reduce the background from other τ decays. Each track associated with the K_S^0 must have $p > 1$ GeV and must not have any hits in the axial regions of the vertex drift chamber, which extends radially from 10.3 to 16.2 cm. If the radial distance to the secondary vertex is between 30 and 150 cm, tracks with hits in the stereo region of the vertex drift chamber, which extends radially from 18.8 to 21.3 cm, are rejected.

Candidate decays containing photon conversions identified with an algorithm described in [10], are rejected. Finally, the mass of the jet (assuming that the primary track is a pion) must be less than 2 GeV and the invariant mass of the K_S^0 candidate is required to be between 0.4 and 0.6 GeV, see fig. 1(d). A total of 349 candidates are obtained with a background of approximately 10%, consisting primarily of $\tau^- \to \rho(770)^- \nu_\tau$ and $\tau^- \to a_1(1260)^- \nu_\tau$ decays.

The sample of $\tau^- \to X^- \overline{K}^0 \nu_\tau$ decays is subdivided into two sets: one in which the primary track is identified as a pion and another in which the primary track is identified as a kaon, as described in section 3. In fig. 2(b), the difference of the pion (P_π) and kaon (P_K) probability weight ratios is shown for tracks identified as charged pions and kaons. A decay is considered to contain a π^- if $P_\pi > P_K$.

A neural network algorithm is used to identify the $\tau^- \to \pi^- \overline{K}^0 \nu_\tau$ and $\tau^- \to \pi^- \overline{K}^0 [\geq 1\pi^0] \nu_\tau$ decay modes. The neural network algorithm is similar to the one used in the K_L^0 analysis; the differences are due to the different topologies of the two selections. The neural network algorithm for this selection uses 6 variables to identify the τ jets:

- The total energy of the jet in the electromagnetic calorimeter divided by the scalar sum of the momenta of the tracks, E/p.

- The number of clusters in the electromagnetic calorimeter with energy greater than 1 GeV in the jet.

- The minimum fraction of active lead glass blocks which together contains more than 90% of the total electromagnetic energy of the jet, F_{90}.

- The total presampler multiplicity in the jet.

- The difference in theta ($\Delta\theta$) and phi ($\Delta\phi$) between the vector obtained by adding together all the tracks and the vector obtained by adding together all the clusters in the electromagnetic calorimeter associated to the jet.

The variables used in the neural network algorithm are shown in figs. 4(a-f). A decay is considered to contain a π^0 if the neural network output, shown in fig. 4(g), is greater than 0.5.

5 Branching ratios

The branching ratios of the $\tau^- \to \pi^- \overline{K}^0 \nu_\tau$, $\tau^- \to \pi^- \overline{K}^0[\geq 1\pi^0]\nu_\tau$ and $\tau^- \to K^- K^0[\geq 0\pi^0]\nu_\tau$ decay modes are calculated independently for the τ jets containing K_L^0 and K_S^0 decays. However, for a given data sample, the three branching ratios are calculated simultaneously. Each selection can be characterised in terms of the efficiency for detecting each decay mode i, the branching ratio of each mode and the number of events selected in the data:

$$\epsilon_{i1}B_1 + \epsilon_{i2}B_2 + \epsilon_{i3}B_3 + \sum_{k=4}^{M} \epsilon_{ik}B_k = \frac{N_i - N_i^{\text{non}-\tau}}{N_\tau(1 - f^{\text{non}-\tau})}$$

where N_i is the number of data events that pass the selection i, ϵ_{ij} ($j = 1, 3$) are the efficiencies for selecting signal j using selection i, ϵ_{ik} ($k = 4, \ldots, M$) are the efficiencies for selecting the τ background modes using selection i and M is the number of the τ decay modes. The branching ratios of the signal channels and backgrounds are B_j ($j = 1, 3$) and B_k ($k = 4, \ldots, M$), respectively. The fraction of non-τ events in the τ pair sample is $f^{\text{non}-\tau}$, N_τ is the total number of taus in the data that pass the τ pair selection and $N_i^{\text{non}-\tau}$ is the non-τ background present in each selection i. The selection efficiencies (ϵ_{ij}) for both signal and background are determined from Monte Carlo simulation. The τ background branching ratios are taken from the Particle Data Group compilation [11].

Solving the three simultaneous equations yields the branching ratios in each sample of selected events. A small correction is applied to the branching ratios to account for any biases introduced into the τ pair sample by the τ pair selection. The bias factor is defined as the ratio of the fraction of the selected decays in a sample of τ decays after the τ selection is applied to the fraction before the selection. The bias factors are calculated using approximately 2.2 million simulated $\tau^+\tau^-$ events. The bias factors for the $\tau^- \to \pi^- \overline{K}^0 \nu_\tau$, $\tau^- \to \pi^- \overline{K}^0[\geq 1\pi^0]\nu_\tau$ and $\tau^- \to K^- K^0[\geq 0\pi^0]\nu_\tau$ decays are found to be 0.99 ± 0.01, 1.00 ± 0.01 and 1.00 ± 0.01 for the branching ratios obtained from the K_L^0 sample, and 0.99 ± 0.01, 1.01 ± 0.03 and 0.99 ± 0.02 for the branching ratios obtained from the K_S^0 sample. The uncertainties on the measurements are statistical only.

The K_L^0 (K_S^0) selection identifies 178 (199) $\tau^- \to \pi^- \overline{K}^0 \nu_\tau$ decays, 81 (67) $\tau^- \to \pi^- \overline{K}^0[\geq 1\pi^0]\nu_\tau$ decays and 41 (83) $\tau^- \to K^- K^0[\geq 0\pi^0]\nu_\tau$ decays. The efficiency matrix for each sample is given in table 1.

The branching ratios obtained from the K_L^0 sample are

$$
\begin{aligned}
B(\tau^- \to \pi^- \overline{K}^0 \nu_\tau) &= (9.1 \pm 0.9 \pm 0.6) \times 10^{-3}, \\
B(\tau^- \to \pi^- \overline{K}^0[\geq 1\pi^0]\nu_\tau) &= (3.6 \pm 1.3 \pm 1.0) \times 10^{-3}, \\
B(\tau^- \to K^- K^0[\geq 0\pi^0]\nu_\tau) &= (3.3 \pm 0.9 \pm 0.7) \times 10^{-3},
\end{aligned}
$$

while the branching ratios obtained from the K_S^0 sample are

$$
\begin{aligned}
B(\tau^- \to \pi^- \overline{K}^0 \nu_\tau) &= (9.6 \pm 1.0 \pm 0.7) \times 10^{-3}, \\
B(\tau^- \to \pi^- \overline{K}^0[\geq 1\pi^0]\nu_\tau) &= (3.0 \pm 0.9 \pm 0.9) \times 10^{-3}, \\
B(\tau^- \to K^- K^0[\geq 0\pi^0]\nu_\tau) &= (3.3 \pm 0.7 \pm 0.5) \times 10^{-3},
\end{aligned}
$$

where the first error is statistical and the second is systematic.

6 Systematic errors

The systematic uncertainties on the branching ratios are presented in table 2. The dominant contributions to the systematic uncertainty arises from the efficiency of the two selections, the uncertainty of the backgrounds, the modelling of the dE/dx, the identification of the π^0 and the modelling of Monte Carlo. These uncertainties are discussed in more detail below. In addition, there are straightforward contributions from the limited statistics of the Monte Carlo samples used to estimate the selection efficiencies and from the uncertainties on the bias factors. The systematic error on the branching ratios due to the Monte Carlo statistics is calculated directly from the statistical uncertainties on the elements of the inverse efficiency matrix [12]. The systematic error on each branching ratio due to the bias factor is calculated directly from the bias factor error.

K_L^0 and K_S^0 selection efficiencies:

The K_L^0 selection efficiency is sensitive to the calibration of the momentum, the energy measured by the hadron calorimeter and the resolution of the hadron calorimeter. The uncertainty on the momentum scale is typically better than 1% [7]. The uncertainty in the energy scale of the hadron calorimeter is obtained by studying a sample of single charged hadrons from τ decays, the level of agreement between the data and Monte Carlo is 1.5%. The uncertainty due to the measurement of the resolution of the hadron calorimeter is estimated by varying the resolution within its uncertainties. Also, the shower containment is examined by looking at the leakage of energy out of the back of the hadron calorimeter. It is found that about 8% of K_L^0 decays may not be fully contained, these decays are well modelled by the Monte Carlo and does not result in a systematic uncertainty.

The K_S^0 selection efficiency is sensitive to the requirements on the impact parameter, the momentum and the number of hits in the stereo and axial regions of the vertex chamber on the tracks associated to the K_S^0 . The systematic error on the K_S^0 selection efficiency is determined by dropping each relevant criterion except for the impact parameter resolution. The impact parameter resolution has been shown to have an uncertainty that is typically better than $\pm 20\%$ [8]. Variations of the impact parameter resolution are found to have almost no contribution to the systematic error on the K_S^0 selection efficiency.

Background estimation:

The systematic error due to the background in the K_L^0 sample includes the uncertainty in the branching ratios of the background decays, including the $\tau^- \to \pi^- \overline{K}^0 K^0 \nu_\tau$ and $\tau^- \to \pi^- \overline{K}^0 K^0 \pi^0 \nu_\tau$ decays, as well as the uncertainty from the Monte Carlo statistics [11,13]. The non-K^0 background consists primarily of π^-, $\rho(770)^-$ and $a_1(1260)^-$ decays in which the decays have a low momentum track with at least one of the final π mesons leaving some energy in the hadron calorimeter. To investigate this background, the K_L^0 selection cut S_H is reversed and the invariant mass spectra are studied for each decay mode. The ratios of the data to the Monte Carlo simulation are consistent with unity: 0.97 ± 0.02, 1.04 ± 0.02 and 0.94 ± 0.06 for the $\pi^- \overline{K}^0$, $\pi^- \overline{K}^0 \geq 1\pi^0$ and $K^- K^0 \geq 0\pi^0$ selections, respectively. The various contributions to the systematic error from the background are added in quadrature.

The background in the K_S^0 sample includes $\tau^- \to \pi^- \overline{K}^0 K^0 \nu_\tau$ and $\tau^- \to \pi^- \overline{K}^0 K^0 \pi^0 \nu_\tau$ decays,

which contain K_S^0 mesons, and other τ decays, the uncertainty is composed of the Monte Carlo statistical uncertainty plus a component due to the uncertainty in the branching ratios of these decays [11, 13]. A study of the sidebands of the $m_{\pi\pi}$ distribution (see fig. 1(d)) showed that the background prediction from other τ decays is observed to be about 20% smaller in the Monte Carlo simulation than in the data. As a result, the background is scaled upward by a factor of 1.2 and a 20% uncertainty is assigned to the background estimate. The background estimate is cross-checked using the invariant mass distributions of the tracks associated with the K_S^0 candidate for each of the exclusive channels. The ratios of the data to the Monte Carlo simulation are consistent: 1.07 ± 0.12, 1.09 ± 0.06 and 0.93 ± 0.11 for the $\pi^- \overline{K}_S^0$, $\pi^- \overline{K}_S^0 \geq 1\pi^0$ and $K^- K_S^0 \geq 0\pi^0$ selections, respectively. The various contributions to the systematic error from the background are added in quadrature.

Modelling of dE/dx:

For both samples, the normalized dE/dx distributions are studied using the sample of single charged hadrons from τ decays. The uncertainty in the branching ratios is estimated by varying the means of the normalised dE/dx distributions by ± 1 standard deviation of their central values. In addition, to account for possible differences in the dE/dx resolution, the widths of the normalized dE/dx distributions are varied by $\pm 30\%$. Due to the three tracks present in the K_S^0 sample, an additional contribution to the systematic error is obtained by measuring the difference in the branching ratios when two different corrections are applied to the Monte Carlo. The first correction is estimated from the one-prong hadronic tau decays while the second correction is estimated using the sample of pions from the decay of the K_S^0. The various contributions to the systematic error from the dE/dx modelling are added in quadrature.

Identification of π^0:

Both the K_L^0 and K_S^0 samples use a neural network algorithm to separate the $\tau^- \to \pi^- \overline{K}^0 \nu_\tau$ and $\tau^- \to \pi^- \overline{K}^0 [\geq 1\pi^0] \nu_\tau$ decay modes. The most powerful variable for distinguishing between these two decays is the energy deposited in the electromagnetic calorimeter. The systematic error in the branching ratio is evaluated by shifting the electromagnetic energy scale by $\pm 1\%$; this variation is assigned after studying the differences between data and Monte Carlo in E/p distributions for 3-prong τ decays.

The uncertainty affecting the π^0 identification also includes the maximum uncertainty when each variable (except in those which include the electromagnetic energy) is individually dropped from the neural network algorithm. These uncertainties are added in quadrature with those obtained from the energy scale uncertainty. The stability of the neural network algorithm is studied by removing all but the two most significant variables from the neural network, the results are within the systematic uncertainties for both samples. As a cross check, the cut on the neural network output for both the K_L^0 and K_S^0 samples is varied between 0.1 and 0.8, with the result being consistent within the total systematic uncertainties.

Monte Carlo modelling:

The models used in the Monte Carlo generator can effect both the pion and kaon momentum spectra. This effect can produce biases when determining the K^0 identification efficiency, the K/π separation and the π^0 identification. The dynamics of the $\pi^- \overline{K}^0$ decay mode are well understood. The $\pi^- \overline{K}^0$ decay mode is generated by Tauola via the $K^*(892)^-$ resonance. The

K^-K^0 final state is generated by Tauola using phase space only.

The $\tau^- \to \pi^-\overline{K}^0[\geq 1\pi^0]\nu_\tau$ decay mode is composed of $\tau^- \to \pi^-\overline{K}^0\pi^0\nu_\tau$ and $\tau^- \to \pi^-\overline{K}^0\pi^0\pi^0\nu_\tau$ decays. The $\tau^- \to \pi^-\overline{K}^0\pi^0\nu_\tau$ channel is modelled by Tauola assuming that the decay proceeds via the $K_1(1400)$ resonance. Recent results from ALEPH [14] on one-prong τ decays with kaons, and OPAL [15] using $\tau^- \to K^-\pi^-\pi^+\nu_\tau$ decays, suggest that the $\tau^- \to \pi^-\overline{K}^0\pi^0\nu_\tau$ decay will also proceed via the $K_1(1270)$ resonance. A special Monte Carlo simulation is generated in which the final state is created using the $K_1(1270)$ and $K_1(1400)$ resonances, using the algorithm developed for the analysis described in [15]. The selection efficiency of the $\tau^- \to \pi^-\overline{K}^0\pi^0\nu_\tau$ final state is estimated from the special Monte Carlo for both resonances. For the K^0_L analysis, the efficiencies agree at a level of 10%. For the K^0_S analysis, the selection efficiencies agree at a level of 5%.

The $\tau^- \to \pi^-\overline{K}^0\pi^0\pi^0\nu_\tau$ decay mode is not modelled by Tauola. The branching ratio of this mode was recently measured to be $(0.26 \pm 0.24) \times 10^{-3}$ [13]. A special Monte Carlo sample of the $\tau^- \to \pi^-\overline{K}^0\pi^0\pi^0\nu_\tau$ decay mode is generated using flat phase space and it is found that the efficiency of the $\tau^- \to \pi^-\overline{K}^0\pi^0\pi^0\nu_\tau$ decay mode agrees within 30% of the efficiency of the $\tau^- \to \pi^-\overline{K}^0\pi^0\nu_\tau$ decay mode. For the systematic uncertainty associated with this decay mode, 30% of the $\tau^- \to \pi^-\overline{K}^0\pi^0\pi^0\nu_\tau$ branching ratio is used.

The $\tau^- \to K^-K^0[\geq 1\pi^0]\nu_\tau$ decay mode is composed of $\tau^- \to K^-K^0\pi^0\nu_\tau$ and $\tau^- \to K^-K^0\pi^0\pi^0\nu_\tau$ decays. The $\tau^- \to K^-K^0\pi^0\nu_\tau$ decay mode is generated by Tauola through a combination of the $\rho(1700)$ and $a_1(1260)$ resonances. Monte Carlo simulations of these two modes are generated separately, again using the algorithm developed for the analysis described in [15]. The selection efficiencies of the $\tau^- \to K^-K^0\pi^0\nu_\tau$ decay mode are calculated for these two samples and are equivalent within statistical errors. No systematic uncertainty is included for this channel. The $\tau^- \to K^-K^0\pi^0\pi^0\nu_\tau$ decay mode is not modelled by Tauola. The Particle Data Group [11] give an upper bound of 0.18×10^{-3} for this channel. A special Monte Carlo sample of the $\tau^- \to K^-K^0\pi^0\pi^0\nu_\tau$ decay mode is generated using flat phase space and the efficiency of the $\tau^- \to K^-K^0\pi^0\pi^0\nu_\tau$ decay mode is observed to be within 30% of the efficiency of the $\tau^- \to K^-K^0\pi^0\nu_\tau$ decay mode. For the systematic uncertainty associated with this decay mode, 30% of the $\tau^- \to K^-K^0\pi^0\pi^0\nu_\tau$ branching ratio is used.

Finally, the $\tau^- \to K^-K^0[\geq 1\pi^0]\nu_\tau$ selection efficiency may depend on the relative $\tau^- \to K^-K^0\nu_\tau$ and $\tau^- \to K^-K^0\pi^0\nu_\tau$ branching ratios. Using the current world averages from [11], the relative contribution of each channel is varied by $\pm 25\%$. For the K^0_S analysis, no effect is observed on the branching ratio, as the efficiency for selecting the two channels is very similar; hence, no systematic error is included.

7 Summary

The branching ratios of the decays of the τ leptons to neutral kaons are measured using the OPAL data recorded at centre-of-mass energies near the Z^0 resonance from a recorded luminosity of 163 pb^{-1}. The measurement is based on two samples which identify τ decays with K^0_L

and K_S^0 mesons. The branching ratios obtained from the K_L^0 sample are

$$
\begin{aligned}
B(\tau^- \to \pi^- \overline{K}^0 \nu_\tau) &= (9.1 \pm 0.9 \pm 0.6) \times 10^{-3}, \\
B(\tau^- \to \pi^- \overline{K}^0 [\geq 1\pi^0] \nu_\tau) &= (3.6 \pm 1.3 \pm 1.0) \times 10^{-3}, \\
B(\tau^- \to K^- K^0 [\geq 0\pi^0] \nu_\tau) &= (3.3 \pm 0.9 \pm 0.7) \times 10^{-3},
\end{aligned}
$$

while the branching ratios obtained from the K_S^0 sample are

$$
\begin{aligned}
B(\tau^- \to \pi^- \overline{K}^0 \nu_\tau) &= (9.6 \pm 1.0 \pm 0.7) \times 10^{-3}, \\
B(\tau^- \to \pi^- \overline{K}^0 [\geq 1\pi^0] \nu_\tau) &= (3.0 \pm 0.9 \pm 0.9) \times 10^{-3}, \\
B(\tau^- \to K^- K^0 [\geq 0\pi^0] \nu_\tau) &= (3.3 \pm 0.7 \pm 0.5) \times 10^{-3}.
\end{aligned}
$$

In each case the first error is statistical and the second systematic. The combined results are

$$
\begin{aligned}
B(\tau^- \to \pi^- \overline{K}^0 \nu_\tau) &= (9.33 \pm 0.68 \pm 0.49) \times 10^{-3}, \\
B(\tau^- \to \pi^- \overline{K}^0 [\geq 1\pi^0] \nu_\tau) &= (3.24 \pm 0.74 \pm 0.66) \times 10^{-3}, \\
B(\tau^- \to K^- K^0 [\geq 0\pi^0] \nu_\tau) &= (3.30 \pm 0.55 \pm 0.39) \times 10^{-3}.
\end{aligned}
$$

The branching ratios are compared with existing measurements and theoretical predictions in fig. 5 for the $\tau^- \to \pi^- \overline{K}^0 \nu_\tau$ and $\tau^- \to \pi^- \overline{K}^0 [\geq 1\pi^0] \nu_\tau$ decay modes [14, 16]. The solid band is the new average branching ratio of the OPAL, ALEPH, CLEO and L3 measurements. The results of this work are in good agreement with previous measurements.

The branching ratios of the decay modes are predicted from various theoretical models. The measurement of the decay fraction of the $\tau^- \to \pi^- \overline{K}^0 \nu_\tau$ decay agrees well with the range $(8.9 - 10.3) \times 10^{-3}$ estimated by Braaten *et al.* in [17] and falls in the range of $(6.6 - 9.6) \times 10^{-3}$ predicted by Finkemeier and Mirkes in [18]. The decay $\tau^- \to \pi^- \overline{K}^0 [\geq 1\pi^0] \nu_\tau$, assuming that the decay contains only one π^0, is predicted to be in the range of $(0.9 - 3.7) \times 10^{-3}$ from [17] and in the range of $(8.1 - 9.6) \times 10^{-3}$ from [18]. The $\tau^- \to \pi^- \overline{K}^0 \pi^0 \nu_\tau$ branching ratio prediction by Finkemeier and Mirkes is significantly higher than the experimental results, however they argue that the widths of the K_1 resonance [11] used in their calculation are unusually narrow and that increasing the K_1 width would give a prediction that agrees with the experimental measurements [19].

The branching ratio of the $\tau^- \to K^- K^0 [\geq 0\pi^0] \nu_\tau$ decay mode is the sum of the $\tau^- \to K^- K^0 \nu_\tau$ and $\tau^- \to K^- K^0 \pi^0 \nu_\tau$ decay modes. The decay fraction agrees well with the estimated range $(2.4 - 4.0) \times 10^{-3}$ predicted by [17] and $(2.3 - 2.7) \times 10^{-3}$ predicted by [18].

The $\tau^- \to \pi^- \overline{K}^0 \nu_\tau$ decay mode is assumed to be dominated by the $K^*(892)^-$ resonance. This can be observed from the $\pi^- \overline{K}^0$ invariant mass distributions shown in fig. 6, for the decay modes $\tau^- \to \pi^- \overline{K}_S^0 \nu_\tau$ and $\tau^- \to \pi^- \overline{K}_L^0 \nu_\tau$, respectively. Assuming that the $\tau^- \to \pi^- \overline{K}^0 \nu_\tau$ decay mode proceeds entirely through the $K^*(892)^-$ resonance, then using isospin invariance the branching ratio of the $\tau^- \to K^*(892)^- \nu_\tau$ decay mode is calculated to be 0.0140 ± 0.0013. This value is consistent with the current world average 0.0128 ± 0.0008 [11].

Finally, the ratio of the decay constants f_ρ and f_{K^*} can be estimated using the $\tau^- \to K^*(892)^- \nu_\tau$ branching ratio and the OPAL $\tau^- \to h^- \pi^0 \nu_\tau$ branching ratio of 0.2589 ± 0.0034 [7]. The $\tau^- \to h^- \pi^0 \nu_\tau$ decay mode is the sum of the decay modes $\tau^- \to \pi^- \pi^0 \nu_\tau$ and $\tau^- \to K^- \pi^0 \nu_\tau$.

The branching ratio of the τ to the final state $\mathrm{K}^-\pi^0\nu_\tau$ is calculated to be $(4.67 \pm 0.42) \times 10^{-3}$ using isospin invariance and the $\tau^- \to \pi^- \overline{\mathrm{K}}^0 \nu_\tau$ branching ratio. Consequently, $B(\tau^- \to \pi^-\pi^0\nu_\tau)$ is derived to be 0.2543 ± 0.0034. Using these results, $\tan\theta_c = 0.227$ for the Cabibbo angle and the particle masses from [11], the decay constant ratio

$$\frac{f_\rho}{f_{\mathrm{K}^*}} = \tan\theta_c \sqrt{\frac{B(\tau^- \to \rho^-\nu_\tau)}{B(\tau^- \to \mathrm{K}^*(892)^-\nu_\tau)}} \left(\frac{m_\tau^2 - m_{\mathrm{K}^*}^2}{m_\tau^2 - m_\rho^2}\right) \sqrt{\frac{m_\tau^2 + 2m_{\mathrm{K}^*}^2}{m_\tau^2 + 2m_\rho^2}} = 0.93 \pm 0.05$$

is obtained. The error is dominated by the uncertainties on the branching ratios. The recent result from ALEPH [13], 0.94 ± 0.03, agrees well with the new OPAL result. Finally, this ratio has been predicted by Oneda [20] using the Das-Mathur-Okubo sum rule relations [21] between the spectral functions based on assumptions of $SU(3)_f$ symmetry. At the $SU(3)_f$ symmetry limit ($m_\mathrm{u} = m_\mathrm{d} = m_\mathrm{s}$), the decay constant ratio is expected to be unity, $f_\rho = f_{\mathrm{K}^*}$. In the asymptotic $SU(3)_f$ symmetry limit at high energies, Oneda predicts that $f_\rho/f_{\mathrm{K}^*} = m_\rho/m_{\mathrm{K}^*} = 0.86$.

Acknowledgements

References

[1] OPAL Collaboration, K. Ahmet *et al.*, Nucl. Instr. and Meth. **A305** (1991) 275;
P.P. Allport *et al.*, Nucl. Instr. and Meth. **A324** (1993) 34;
P.P. Allport *et al.*, Nucl. Instr. and Meth. **A346** (1994) 476.

[2] M. Hauschild *et al.*, Nucl. Instr. and Meth. **A314** (1992) 74;
O. Biebel *et al.*, Nucl. Instr. and Meth. **A323** (1992) 169;
M. Hauschild, Nucl. Instr. and Meth. **A379** (1996) 436.

[3] S. Jadach, B.F.L. Ward, and Z. Wąs, Comp. Phys. Comm. **79** (1994) 503.

[4] S. Jadach *et al.*, Comp. Phys. Comm. **76** (1993) 361.

[5] J. Allison *et al.*, Nucl. Inst. and Meth. **A317** (1992) 47.

[6] OPAL Collaboration, G. Alexander *et al.*, Phys. Lett. **B369** (1996) 163.

[7] OPAL Collaboration, K. Ackerstaff *et al.*, Eur. Phys. J. **C4** (1998) 193.

[8] OPAL Collaboration, K. Ackerstaff *et al.*, Eur. Phys. J. **C8** (1999) 183.

[9] OPAL Collaboration, R. Akers *et al.*, Z. Phys. **C67** (1995) 389.

[10] OPAL Collaboration, G. Alexander *et al.*, Z. Phys. **C70** (1996) 357.

[11] Particle Data Group, C. Caso *et al.*, Eur. Phys. J. **C3** (1998) 1.

[12] M. Lefebvre, R.K. Keeler, R. Sobie and J. White, *Propagation of Errors for Matrix Inversion*, hep-ex/9909031, Submitted to Nucl. Inst. and Meth.

[13] ALEPH Collaboration, R. Barate *et al.*, *Study of Tau Decays Involving Kaons, Spectral Functions and Determination of the Strange Quark Mass*, CERN-EP/99-026.

[14] ALEPH Collaboration, R. Barate *et al.*, Eur. Phys. J., **C10** (1999) 1.

[15] OPAL Collaboration, G. Abbiendi *et al.*, *A Study of three Prong Tau Decays with Charged Kaons*, CERN-EP/99-095.

[16] ALEPH Collaboration, R. Barate *et al.*, Eur. Phys. J., **C4** (1998) 29;
L3 Collaboration, M. Acciarri *et al.*, Phys. Lett. **B352** (1995) 487;
CLEO Collaboration, T.E. Coan *et al.*, Phys. Rev. **D53** (1996) 6037.

[17] E. Braaten, R. Oakes and S. Tse, Int. J. Mod. Phys., **A5** (1990) 2737.

[18] M. Finkemeier and E. Mirkes, Z.Phys., **C69** (1996) 243.

[19] M. Finkemeier, J.H. Kühn and E. Mirkes, Nucl. Phys. Proc. Suppl. **C55** (1997) 169.

[20] S. Oneda, Phys. Rev. **D35** (1987) 397;
T. Matsuda and S. Oneda, Phys. Rev. **171** (1968) 1743.

[21] T. Das, V.S. Mathur and S. Okubo, Phys. Rev. Lett. **18** (1967) 761;
T. Das, V.S. Mathur and S. Okubo, Phys. Rev. Lett. **19** (1967) 859.

Table 1: Signal efficiencies for each selection relative to selecting a K^0. The errors on these efficiencies are based on Monte Carlo statistics only. The first column lists the three selection classes. The three remaining columns give the Monte Carlo selection efficiency for a decay of the indicated type passing that selection classification.

Selection	Selection efficiency from MC (%)		
	$\tau^- \to \pi^- \overline{K}^0 \nu_\tau$	$\tau^- \to \pi^- \overline{K}^0 [\geq 1\pi^0] \nu_\tau$	$\tau^- \to K^- K^0 [\geq 0\pi^0] \nu_\tau$
K_L^0 sample			
$\pi^- \overline{K}^0$	7.36 ± 0.18	0.81 ± 0.09	0.28 ± 0.06
$\pi^- \overline{K}^0 [\geq 1\pi^0]$	1.05 ± 0.07	3.60 ± 0.19	0.08 ± 0.03
$K^- K^0 [\geq 0\pi^0]$	0.43 ± 0.05	0.19 ± 0.04	3.53 ± 0.21
K_S^0 sample			
$\pi^- \overline{K}^0$	8.94 ± 0.18	2.88 ± 0.18	1.46 ± 0.13
$\pi^- \overline{K}^0 [\geq 1\pi^0]$	0.48 ± 0.05	5.32 ± 0.24	0.27 ± 0.06
$K^- K^0 [\geq 0\pi^0]$	0.99 ± 0.07	0.93 ± 0.10	8.44 ± 0.29

Table 2: Systematic errors on the branching ratios.

	Branching ratio systematic errors ($\times 10^{-3}$) for the K_L^0 selection		
	$B(\tau^- \to \pi^- \overline{K}^0 \nu_\tau)$	$B(\tau^- \to \pi^- \overline{K}^0 [\geq 1\pi^0] \nu_\tau)$	$B(\tau^- \to K^- K^0 [\geq 0\pi^0] \nu_\tau)$
MC statistics	0.24	0.28	0.24
Bias factor	0.14	0.05	0.05
K_L^0 efficiency	0.40	0.68	0.42
Background	0.29	0.50	0.31
dE/dx modelling	0.21	0.11	0.33
π^0 efficiency	0.14	0.27	0.00
MC modelling	0.00	0.39	0.17
Total	0.62	1.02	0.68

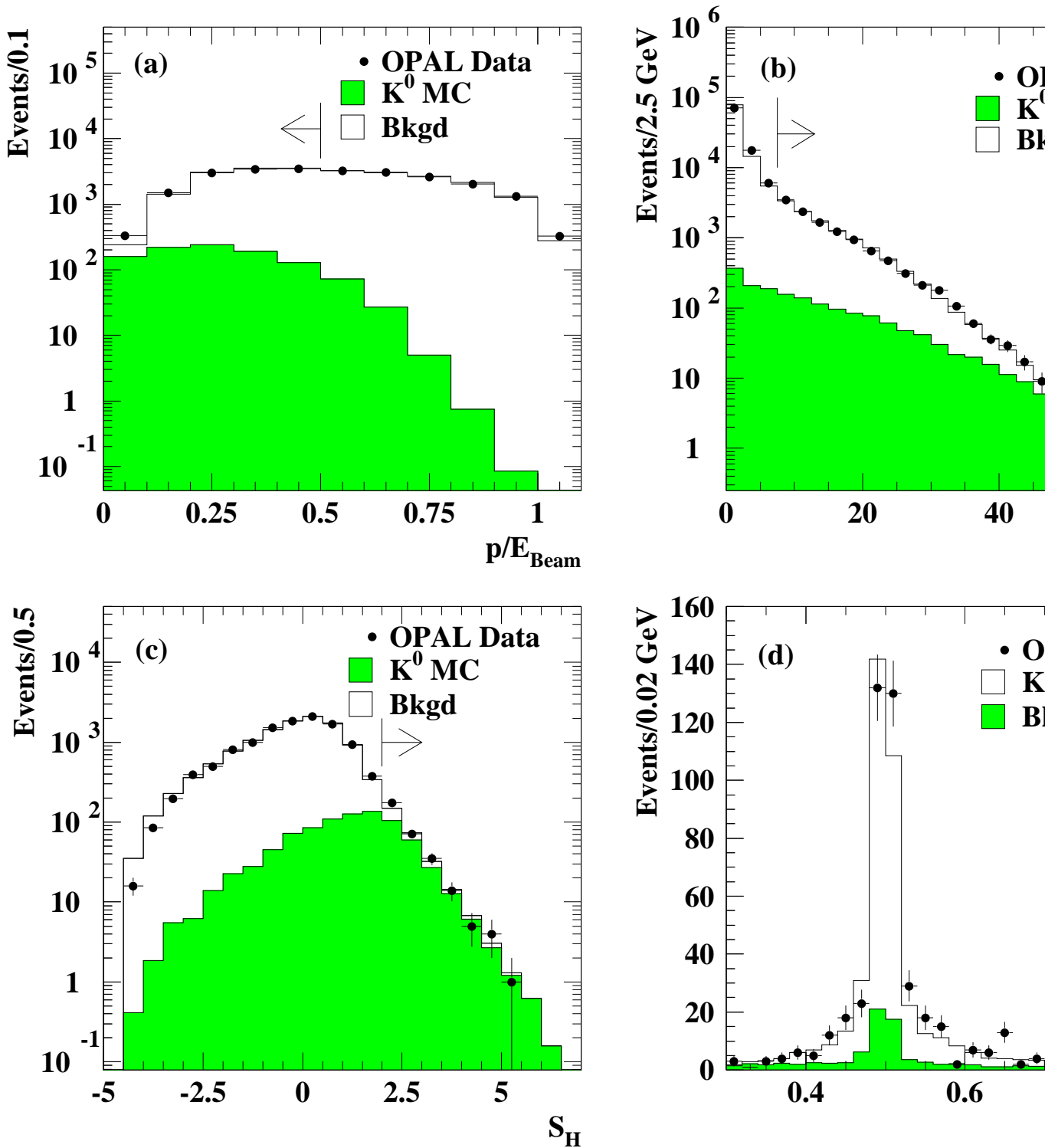|	Branching ratio systematic errors ($\times 10^{-3}$) for the K_S^0 selection		
	$B(\tau^- \to \pi^- \overline{K}^0 \nu_\tau)$	$B(\tau^- \to \pi^- \overline{K}^0 [\geq 1\pi^0] \nu_\tau)$	$B(\tau^- \to K^- K^0 [\geq 0\pi^0] \nu_\tau)$
MC statistics	0.23	0.17	0.15
Bias factor	0.10	0.09	0.07
K_S^0 efficiency	0.46	0.66	0.18
Background	0.40	0.44	0.21
dE/dx modelling	0.26	0.10	0.32
π^0 efficiency	0.22	0.22	0.00
MC modelling	0.00	0.31	0.16
Total	0.74	0.91	0.48

Figure 1: The first three plots show the K_L^0 selection variables: (a) the momentum divided by the beam energy (p/E_{beam}), (b) the hadronic calorimeter energy (E_{HB}) and (c) $S_H = (E_H - p)/\sigma_H$. The fourth plot shows the mass distribution of jets which pass the K_S^0 selection. In each case, jets which pass all of the selection requirements except for the variable in question are plotted.
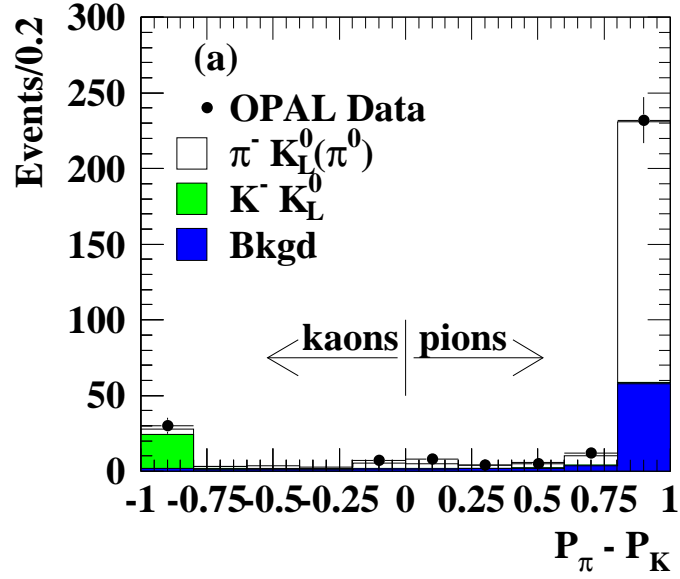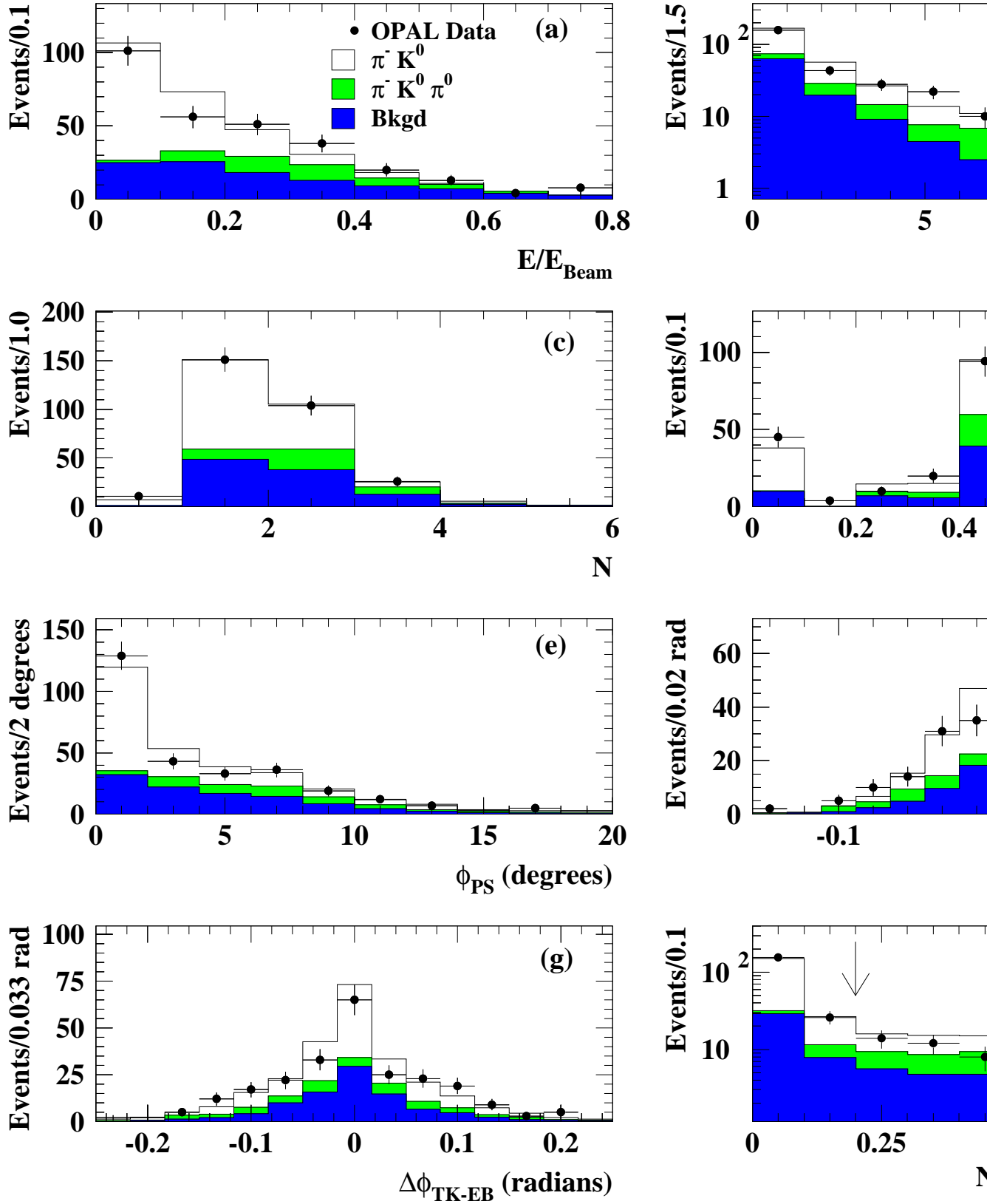
0.75

0.75
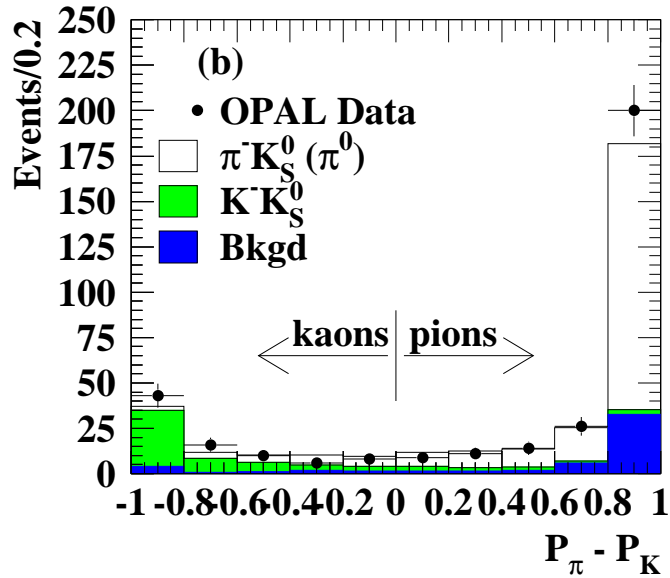
Figure 2: The π/K separation variables. (a) shows the difference of the pion (P_π) and kaon (P_K) probabilities, $P_\pi - P_K$, for the K_L^0 sample, (b) shows $P_\pi - P_K$ for the K_S^0 sample.

17

0.65

Figure 3: The variables used in the neural network routine for identifying π^0 mesons in the K_L^0 sample: (a) the electromagnetic energy divided by the beam energy; (b) the ratio of the electromagnetic energy (E) with the momentum of the track (p); (c) the number of electromagnetic calorimeter clusters (N); (d) the fraction of lead glass blocks in the electromagnetic calorimeter with over 90% of the energy in the jet; (e) angle between the position of the track
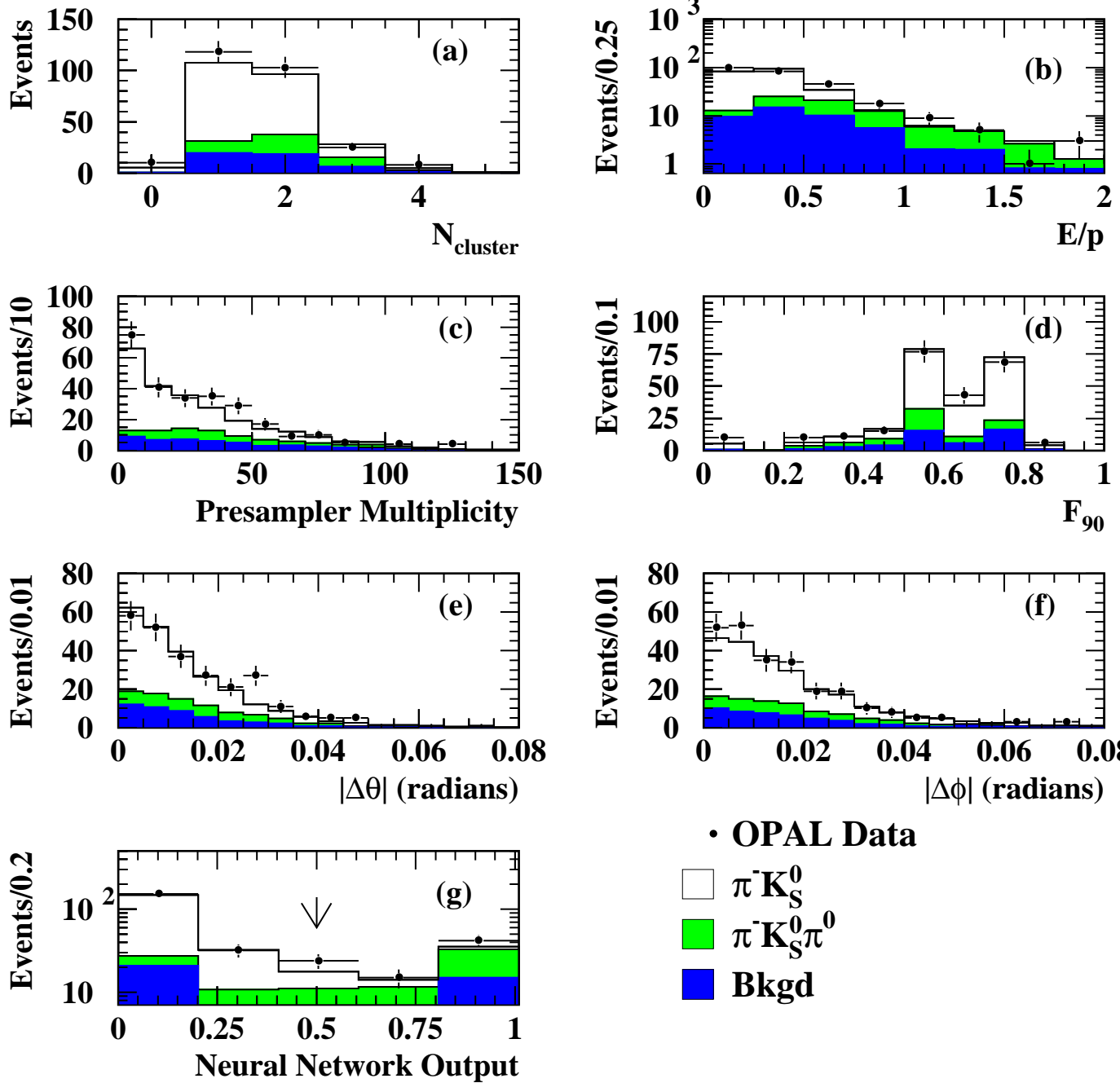
0.80

Figure 4: The variables used in the neural network routine for identifying π^0 mesons in the K_S^0 sample: (a) the number of clusters in the electromagnetic calorimeter; (b) the ratio of the total energy in the electromagnetic calorimeter divided by the total scalar momentum of the tracks; (c) the presampler multiplicity, (d) the fraction of lead glass blocks in the electromagnetic calorimeter with over 90% of the energy in the jet; (e) and (f) the difference in theta ($\Delta\theta$) and phi ($\Delta\phi$) between the vector obtained by adding all the tracks and the vector obtained by adding all the clusters in the electromagnetic calorimeter; (g) the output of the neural network, the arrow indicates the cut used to select decays containing π^0 mesons.
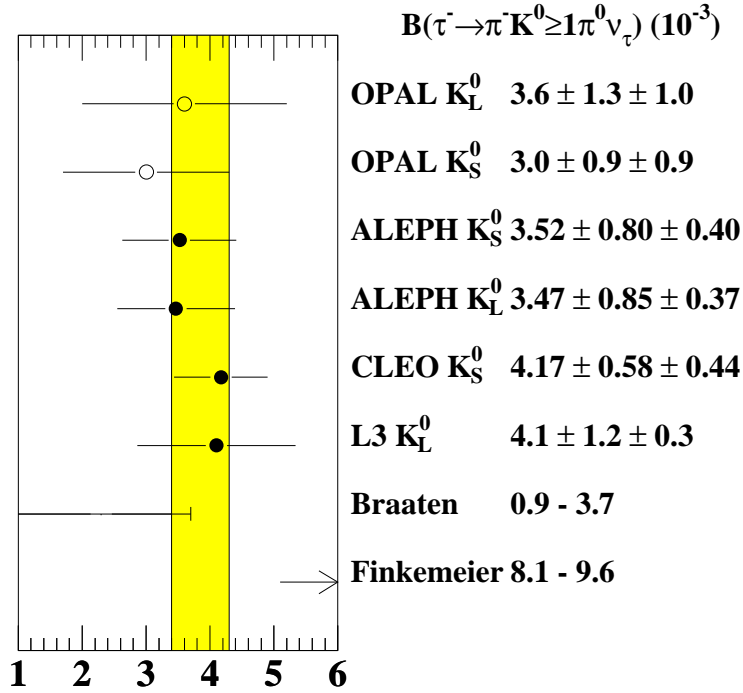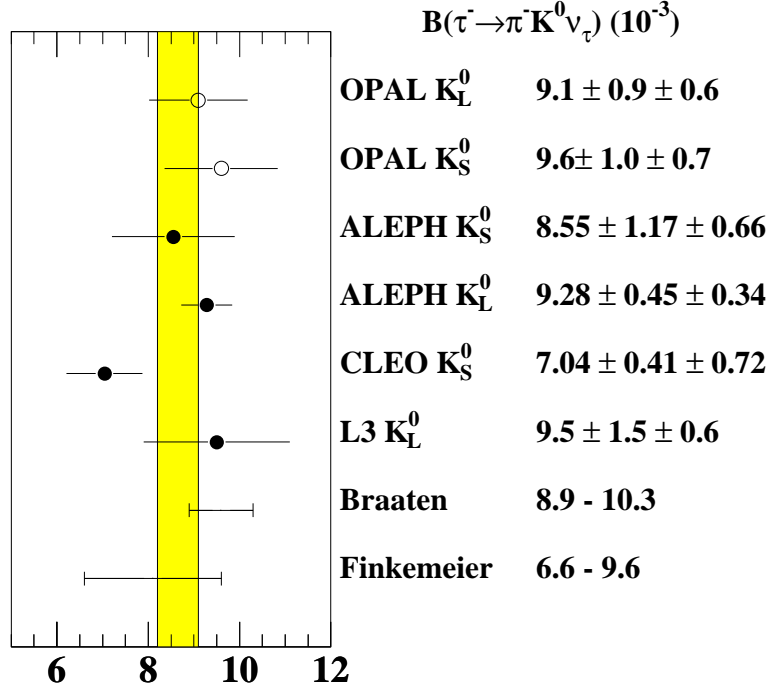
19

B($\tau^- \to \pi^- K^0 \nu_\tau$) ($10^{-3}$)

OPAL K_L^0		$9.1 \pm 0.9 \pm 0.6$
OPAL K_S^0		$9.6 \pm 1.0 \pm 0.7$
ALEPH K_S^0		$8.55 \pm 1.17 \pm 0.66$
ALEPH K_L^0		$9.28 \pm 0.45 \pm 0.34$
CLEO K_S^0		$7.04 \pm 0.41 \pm 0.72$
L3 K_L^0		$9.5 \pm 1.5 \pm 0.6$
Braaten		8.9 - 10.3
Finkemeier		6.6 - 9.6

B($\tau^- \to \pi^- K^0 \geq 1\pi^0 \nu_\tau$) ($10^{-3}$)

OPAL K_L^0	$3.6 \pm 1.3 \pm 1.0$
OPAL K_S^0	$3.0 \pm 0.9 \pm 0.9$
ALEPH K_S^0	$3.52 \pm 0.80 \pm 0.40$
ALEPH K_L^0	$3.47 \pm 0.85 \pm 0.37$
CLEO K_S^0	$4.17 \pm 0.58 \pm 0.44$
L3 K_L^0	$4.1 \pm 1.2 \pm 0.3$
Braaten	0.9 - 3.7
Finkemeier	8.1 - 9.6

Figure 5: Branching ratios of the $\tau^- \to \pi^- \overline{K}^0 \nu_\tau$ and $\tau^- \to \pi^- \overline{K}^0 [\geq 1\pi^0]\nu_\tau$ decays measured or calculated to date. The solid band is the average branching ratio of the OPAL, ALEPH, CLEO and L3 measurements [14, 16]. The $\tau^- \to \pi^- \overline{K}^0 [\geq 1\pi^0]\nu_\tau$ results include both the $\tau^- \to \pi^- \overline{K}^0 \pi^0 \nu_\tau$ and $\tau^- \to \pi^- \overline{K}^0 \pi^0 \pi^0 \nu_\tau$ measurements (ALEPH) and inclusive results (OPAL,L3,CLEO). The theoretical estimates are shown for the $\tau^- \to \pi^- \overline{K}^0 \pi^0 \nu_\tau$ decay mode only [17, 18]. The open points show the new OPAL results, the solid points other experimental results and the bounded lines show two theoretical predicted ranges of the branching fractions.

[scale=.75]pr293$_0$6a.eps[scale = .75]pr293$_0$6b.eps

Figure 6: The $\overline{\mathrm{K}}^0_\mathrm{S}\pi^-$ and $\overline{\mathrm{K}}^0_\mathrm{L}\pi^-$ invariant mass spectra for the the decay channels $\tau^- \to \pi^-\overline{\mathrm{K}}^0_\mathrm{S}\nu_\tau$ and $\tau^- \to \pi^-\overline{\mathrm{K}}^0_\mathrm{L}\nu_\tau$, respectively.